

Bottomonium Hyperfine Splitting on the Lattice and in the Continuum

by

Ahmed Ashraf Rayyan

A thesis submitted in partial fulfillment of the requirements for

the degree of

Master of Science

Department of Physics

University of Alberta

© Ahmed Ashraf Rayyan, 2018

Abstract

In this thesis¹ we study the mass difference between the $1S$ spin-singlet and spin-triplet bottom quark-antiquark bound states within the effective theory of lattice non-relativistic quantum chromodynamics (NRQCD). The precise determination of this value, called the *bottomonium hyperfine splitting*, has been difficult to obtain due to disagreements between phenomenological, lattice, and experimental groups. In particular, the two latest independent lattice determinations’ central values differ beyond their quoted error bars even though they are based on the same bare lattice NRQCD simulation data. However, these two analyses differ in their “*matching*” methods, wherein the parameters of the effective theory are determined. The approach based on the expansion about the continuum limit was introduced in ref. [3] and differs from the standard perturbative matching employed by refs. [4–7]. Using a numerical and analytical solution of the lattice Schrödinger equation, we trace the discrepancy of the two results to a subtle problem regarding the Coulomb binding effects and their lattice artifacts, which leads to a breakdown in the standard perturbative matching unique to lattice regularization. We introduce a new consistent method named “Schrödinger matching,” which performs the matching using the solution of the full Schrödinger equation without an expansion in the Coulomb interaction. Our analysis resolves the discrepancy in favor of the result of ref. [3], which is 52.9 ± 5.5 MeV for the bottomonium hyperfine splitting; this reconciles the two lattice results, along with the perturbative QCD result and the most precise experimental measurements to date.

¹This work is based on refs. [1, 2].

Dedication

To my family: Ashraf, Rasha, and Hams.

Acknowledgements

I would like to thank Alexander Penin for his continual guidance during my research project. I would also like to thank the members of my examining committee for their helpful comments on my thesis: Joseph Maciejko, Frank Marsiglio, and Roger Moore.

Contents

1	Introduction: Hyperfine Splitting in Bottomonium	1
1.1	Heavy Quarkonium	1
1.2	The η_b Mass Puzzle	4
1.3	Outline	5
2	NRQCD on the Lattice and in the Continuum	8
2.1	Motivation	8
2.2	NRQCD Lagrangian	10
2.2.1	Lattice NRQCD	14
2.3	Radiative Improvement and Matching in Lattice NRQCD	16
2.3.1	Expansion About the Continuum Limit	18
2.3.2	Direct Numerical Matching	19
3	Coulomb Binding Effects on the Lattice	21
3.1	Coulomb Binding Effects	21
3.2	Coulomb Artifact to 1-Loop	25
3.3	Coulomb Artifact to All Orders	26
3.4	Breakdown of Perturbative Matching	29
4	Determination of the Energy Spectrum From the Lattice Data	35
4.1	Summary	39

Bibliography	41
Appendix A Feynman Rules of NRQCD	44
Appendix B Spin-Dependent Coulomb NRQCD Amplitudes	46
B.1 Tree-Level	47
B.2 One-Loop	48
Appendix C Solving the Schrödinger Equation on the Lattice	50
C.1 Numerical Approach	52
C.2 Analytical Approach	54

Chapter 1

Introduction: Hyperfine Splitting in Bottomonium

1.1 Heavy Quarkonium

Experiment 288 at Fermilab, led by Leon Lederman, was proposed to study dilepton production as a result of proton-nucleon collisions. The E288 collaboration discovered a dimuon resonance at 9.5 GeV in the summer of 1977, which was the first observation of the Upsilon (Υ) particle [8]. This, along with the discovery of the J/ψ particle in 1974 by SLAC and the Brookhaven National Laboratory simultaneously [9, 10], prompted an extension of the quark model to include the bottom (b) and charm (c) quarks respectively.¹ Here the Υ and J/ψ particles were realized as new types of *quarkonia*, or bound states of a quark and their corresponding antiquark.² The large mass of these new quarkonia suggested that the b and c quarks were much heavier than the already known up, down and strange quarks (u , d , and s , respectively).

In fact, we can give a precise definition of what a heavy quark is if we look at the theory underlying the quark model. Quantum chromodynamics (QCD) is a non-abelian gauge

¹The last quark flavour, the top (t), was discovered in 1995.

²In particular, we call bottom quark-antiquark bound states *bottomonium* ($b\bar{b}$).

theory, invariant under the local action of the gauge group $SU(3)$. It is best conceptualized as a generalization of the $U(1)$ abelian gauge theory quantum electrodynamics (QED), the highly successful quantum theory of electric charges and their interactions via photons. However, the important distinction between QED and QCD is that, in the latter theory, the force carriers (called gluons) transform non-trivially under the action of $SU(3)$: in layman terms, gluons self-interact while photons do not. A related distinction is that, while the creation and annihilation of virtual electron-positron pairs in QED results in a screening of electric charge, virtual gluon self-interactions result in an opposing anti-screening effect. This is best visualized in the coupling constant α of both theories, which is given by the renormalization group equation (to one-loop)

$$Q \frac{d}{dQ} \alpha(Q) = -\frac{\alpha(Q)^2}{2\pi} \beta_0, \quad \beta_0 = \frac{11}{3} C_A - \frac{2}{3} n_f \quad (1.1)$$

where Q is the momentum scale, n_f is the number of fermion flavours in consideration, and C_A is a factor related to the self-interactions of the force carriers in the theory [11]. Now, in QED, $C_A = 0$, resulting in $\beta_0 < 0$; as a result eq. (1.1) predicts the monotonic increasing of $\alpha(Q)$ from 0 and the reliability of a perturbative expansion in α until $\alpha \sim 1$.³ In QCD however, the anti-screening effect of gluons is reflected in the result $C_A = 3$, and as long as the number of fermion flavours does not exceed 16, $\beta_0 > 0$. Thus eq. (1.1) predicts the monotonic *decreasing* of the QCD coupling constant α_s . Solving this equation gives

$$\alpha_s(Q) = \frac{2\pi}{\beta_0 \log(Q/\Lambda_{\text{QCD}})} \quad (1.2)$$

where Λ_{QCD} is the scale at which perturbation theory breaks down. Momentum scales $Q \gg \Lambda_{\text{QCD}}$ are amenable to a perturbative analysis in α_s .

We can now give a definition of the heavy quarks, which include the charm, bot-

³Thankfully, this does not occur until $\Lambda_{\text{QED}} \sim 10^{280}$ MeV: see the discussion on the Landau pole in ref. [11]. Even then, QED is not a good description of electric charges at roughly 80 GeV due to the production of W^\pm and Z bosons.

tom, and top quarks: $m_q \gg \Lambda_{\text{QCD}}$. In principle we could then study heavy quarkonia within the framework of perturbative QCD, usually through the Bethe-Salpeter formalism. However, the dynamics of bound states is a multiscale problem which proves to be intractable within the relativistic QCD framework. Fortunately the quarks in heavy quarkonia have relative velocity $v \ll 1$ due to their heavy masses and small coupling, which gives an additional small parameter to expand in. In the leading order of the expansion, heavy quarkonia is similar to the hydrogen atom in that it is a Coulombic system described by the Schrödinger equation. The further corrections in v are systematically employed using an effective field theory framework, which separates the relativistic scales (computed within QCD) from the non-relativistic modes (which are computed within the effective Schrödinger-like picture). Indeed, the effective field theories “non-relativistic QCD” (NRQCD) and “potential non-relativistic QCD” (pNRQCD) have been successful in achieving a non-relativistic quantum mechanical description of heavy quarkonia from the first principles of Poincare invariance and local gauge symmetry [12].

In order to obtain high-precision results, one must also take into account the contribution of long-distance confinement effects without an expansion in α_s but instead relying on non-perturbative approaches like lattice simulations. In this method the field theory path integral is evaluated numerically on a discrete Euclidean space-time grid; the lattice NRQCD framework then allows the non-relativistic modes to be simulated on the lattice [13, 14]. What we study in our thesis is how the non-perturbative lattice result for the long-distance contributions is consistently combined with the perturbative QCD result for the short-distance contributions in order to produce precise results for heavy quarkonium observables.

1.2 The η_b Mass Puzzle

The quantum theory of spin tells us that a spin-1/2 particle transforms according to the $\mathbf{2}$ representation of $SU(2)$. Then, if we combine a bottom quark and antiquark, the addition of angular momentum implies

$$\mathbf{2} \otimes \mathbf{2} = \mathbf{1} \oplus \mathbf{3},$$

or that the quark-antiquark pair form either a spin-1 triplet (the familiar Υ) or the spin-0 singlet (dubbed the η_b). An interaction between the two spins \mathbf{S}_1 and \mathbf{S}_2 will be proportional to $\mathbf{S}_1 \cdot \mathbf{S}_2$, which induces a mass difference called the *hyperfine splitting*. In bottomonium, the ground state hyperfine splitting is simply defined as

$$E_{\text{hfs}} = M_{\Upsilon(1S)} - M_{\eta_b(1S)}$$

While the triplet (with a PDG mass of 9460.30 ± 0.26 MeV) was first observed in 1977, the singlet is much harder to identify as it can only be excited via weak M1 transitions [8, 16]. Nevertheless, 31 years after the Υ discovery, the η_b was observed by the BaBar collaboration in the radiative decay channel $\Upsilon(3S) \rightarrow \gamma \eta_b(1S)$, and the hyperfine splitting was determined to be $71.4^{+3.5}_{-4.1}$ MeV [17]. However, their analysis contained a systematic error due to the subtraction of an asymmetric background resonance.

On the other hand, the phenomenological pNRQCD prediction for the hyperfine splitting was 41 ± 14 MeV, close to *half* the BaBar value [18]. This was concerning as it demonstrated that perturbative analyses may not be valid for the bottomonium ground state, which was thought to be uncontaminated by confinement effects. To control these nonperturbative contributions, the HPQCD collaboration used lattice NRQCD simulations and obtained 70 ± 9 MeV, favouring the higher value of the hyperfine splitting [6]. Nine months after, the Belle collaboration observed the $\eta_b(1S)$ in the P-wave decay channels $h_b(nP) \rightarrow \gamma \eta_b(1S)$ and released a much lower value of 57.9 ± 2.3 MeV, the most precise experimental determination of the hyperfine splitting so far [19]. Clearly, there

was no convergence to a value for the mass of the η_b , and it became clear that the proper accounting of radiative effects in lattice NRQCD was necessary for a precise determination using lattice simulations.

One approach, developed in refs. [4, 5] and later implemented on the lattice by the HPQCD collaboration, gives a value of 60.0 ± 6.4 MeV, a reduction from their last prediction [7]. A year later, an approach based on the asymptotic expansion about the continuum limit developed in ref. [3] gave a value of 52.9 ± 5.5 MeV. The difference between the two latest results in refs. [3, 7] is larger than one would expect, specifically since they are based on the same bare (ie. non-radiatively improved) lattice data and their respective errors are correlated.⁴ This goal of this thesis is to identify the source of this subtle difference, and determine which method is the proper account of radiative effects of lattice NRQCD.

Result	E_{hfs} (MeV)
Kniehl <i>et al.</i> [18]	41 ± 14
BaBar [17]	$71.4^{+3.5}_{-4.1}$
HPQCD [6]	70 ± 9
Belle [19]	57.9 ± 2.3
HPQCD [7]	60.0 ± 6.4
Baker <i>et al.</i> [3]	52.9 ± 5.5

Table 1.1: Summary of bottomonium hyperfine splitting results

1.3 Outline

The difference between the two approaches of refs. [3] and [4, 5] is related to the description of the lattice Coulomb artifacts resulting from the effect of space discretization on the Coulomb bound state dynamics. The Coulomb artifacts appear as powers of a dimensionless combination $am_q\alpha_s$ (where α_s is the strong coupling constant, a is the lattice spacing, and m_q is the heavy quark mass) in the parameters of the bound states evaluated on the

⁴Specifically, the central values should only differ relatively by $\alpha_s v^2 \sim 2\%$ due to radiative and relativistic corrections.

lattice. This dependence on the lattice spacing should be cancelled in the final result for the physical quarkonium spectrum through the so-called *matching* procedure and an inconsistent treatment of the artifacts may lead to a large systematic error of the lattice NRQCD predictions. In this thesis, by studying both a numerical and explicit analytical solution of the Schrödinger equation on the lattice, we show that the standard finite-order perturbative matching is insufficient in dealing with the Coulomb artifacts [1, 2]. This appears counterintuitive since the lattice regularization is usually associated with a momentum cutoff at the scale a^{-1} much larger than the scale $m_q\alpha_s$ of Coulomb dynamics, and the corresponding short-distance effects are supposed to be systematically described by the standard matching procedure. However, we find that the failure of perturbative matching is a consequence of a fine interplay between the short- and long-distance effects specific to the lattice regularization of NRQCD, and results in the discrepancy between the two latest lattice NRQCD results for the ground state hyperfine splitting of bottomonium [3, 7]. The remainder of the thesis provides the details leading to our findings and is organized as follows.

In Chapter 2, we give a brief introduction to continuum and lattice NRQCD, including the explicit construction of the NRQCD Lagrangian to $\mathcal{O}(v^4)$ accuracy, inclusive. We also introduce two approaches towards the radiative improvement of the NRQCD action: the standard perturbative approach [4, 5] and the approach based on the asymptotic expansion about the continuum limit [3].

In Chapter 3, we discuss the problem with the standard perturbative matching related to the treatment of Coulomb binding effects within lattice NRQCD. We show that these effects result in the breakdown of perturbative matching for the Coulomb lattice artifacts, and we propose a new method termed “Schrödinger matching” which takes into account these terms consistently.

In Chapter 4, we will discuss the effect of the breakdown of perturbative matching on the bottomonium ground state hyperfine splitting. We then conclude by comparing the

result with that of ref. [3], as well as the latest experimental values for the bottomonium hyperfine splitting.

Chapter 2

NRQCD on the Lattice and in the Continuum

2.1 Motivation

The dynamics of quarkonium systems exhibits several scales:¹

- the *hard* scale, on the order of the mass of the quark m_q ,
- the *soft* scale, on the order of the inverse Bohr radius $m_q v$,
- the *ultrasoft* scale, on the order of the kinetic energy $m_q v^2$, and
- the *confinement* scale $\Lambda_{\text{QCD}} \sim 200 \text{ MeV}$ (in the \overline{MS} renormalization scheme).

Let us now specialize to heavy quarkonium, where the constituent quarks have the property $m_q \gg \Lambda_{\text{QCD}}$: the relevant example is the bottomonium system where $m_b \sim 4.2 \text{ GeV}$ in the \overline{MS} scheme [15]. At the same time the energy splittings between the ground and first excited states of bottomonium sets the kinetic energy scale at $m_b v^2 \sim 500 \text{ MeV}$ [20]. The large discrepancy between the two scales suggest that the relative motion of the

¹Unless stated otherwise, we work in “natural” units where $\hbar = c = 1$; in this set of units, distances are measured in inverse mass dimensions.

quarks inside the bottomonium ground state is non-relativistic, and that the quarkonium scales separate into the hierarchy

$$m_q \gg m_q v \gg m_q v^2 \gtrsim \Lambda_{\text{QCD}}$$

Eq. (1.2) suggests that, if some scale is much larger than Λ_{QCD} , then the effects at that scale can be computed using perturbative QCD since $\alpha_s \ll 1$ there. Given that most of the bound state dynamics is set by the Bohr radius, it makes sense to remove the mass scale from the dynamics of the theory and to compute these short-distance effects perturbatively: the result is the effective field theory of non-relativistic QCD (NRQCD), first introduced in refs. [21, 22]. The construction of the theory is done in two steps.

First, we take advantage of the scale hierarchy by introducing a factorization scale μ such that $m_q v \ll \mu \ll m_q$, and *integrating out* all effects greater than μ into the parameters of the new effective theory. This is explicitly done by decoupling the quark and antiquark fields from one another and expanding the resultant equations of motions in powers of v . This generates an infinite number of new NRQCD interactions which, at a given order in v , describes the low-energy dynamics of the bound state. To replicate the effects of quark-antiquark annihilation, it will be necessary to additionally include new *ad hoc* four-fermion contact operators to the effective Lagrangian.

Secondly, we determine the parameters of the new effective theory via *matching*, where we demand that QCD and NRQCD amplitudes coincide order-by-order in v at scales less than the factorization scale μ . These parameters are referred to as *matching* or *Wilson coefficients*. In particular, we will focus on the four-fermion Wilson coefficients, where the interplay between binding effects and lattice regularization give rise to a subtle problem in matching.

2.2 NRQCD Lagrangian

We will now construct the NRQCD Lagrangian using the steps outlined above. In QCD, our fermionic degrees of freedom are given by a single 4-component Dirac spinor Ψ of mass m_q , which has dynamics governed by the Dirac Lagrangian:

$$\mathcal{L}_q = \bar{\Psi} (i\gamma^\mu D_\mu - m_q) \Psi$$

where γ^μ are the Dirac gamma matrices satisfying $\{\gamma^\mu, \gamma^\nu\} = 2g^{\mu\nu}$, $iD_\mu = i\partial_\mu - A_\mu$ is the covariant derivative² and $A_\mu \equiv A_\mu^a T^a$ is the $SU(3)$ gauge field, with T^a being the generators of the $SU(3)$ gauge group. Explicitly, the temporal and spatial components are given as

$$iD^0 = i\partial^0 - A^0, \quad i\mathbf{D} = i\nabla + \mathbf{A}$$

Varying the action $S = \int d^4x \mathcal{L}_q$ with respect to $\bar{\Psi}$ gives the equation of motion

$$(i\gamma^\mu D_\mu - m_q) \Psi = 0 \tag{2.1}$$

Let us now specialize to the heavy quarkonium system with $m_q \gg \Lambda_{\text{QCD}}$, noting that in a non-relativistic bound state, the energy is dominated by the rest mass. Let us then factor out this rapidly oscillating mode by making the shift $\Psi \rightarrow e^{-im_q t} \Psi$; using that

$$i\gamma^0 D_0 (e^{-im_q t} \Psi) = e^{-im_q t} (\gamma^0 m_q + i\gamma^0 D_0) \Psi \tag{2.2}$$

we have

$$[i\gamma^\mu D_\mu + (\gamma^0 - 1) m_q] \Psi = 0 \tag{2.3}$$

²In this thesis, the covariant derivative acts on everything to its right.

Now, in the Dirac representation, the Dirac matrices are given by

$$\gamma^0 = \begin{pmatrix} 1 & 0 \\ 0 & -1 \end{pmatrix} \quad \gamma^i = \begin{pmatrix} 0 & \sigma^i \\ -\sigma^i & 0 \end{pmatrix}$$

where σ^i are the Pauli matrices satisfying

$$[\sigma^i, \sigma^j] = 2i\epsilon^{ijk}\sigma^k, \quad \{\sigma^i, \sigma^j\} = 2\delta^{ij}$$

Let us now separate the 4-component Dirac spinor Ψ into two, 2-component Pauli spinors ψ and χ , representing the large and small components of Ψ respectively. Eq. (2.3) then gives the two coupled equations³

$$\begin{aligned} iD_0\psi - i\boldsymbol{\sigma} \cdot \mathbf{D}\chi &= 0 \\ i\boldsymbol{\sigma} \cdot \mathbf{D}\psi - (iD_0 + 2m_q)\chi &= 0 \end{aligned}$$

Formally we can solve for χ in the second equation, and substitute that into the first:

$$\left(iD_0 - i\boldsymbol{\sigma} \cdot \mathbf{D} \frac{1}{iD_0 + 2m_q} i\boldsymbol{\sigma} \cdot \mathbf{D} \right) \psi = 0 \quad (2.4)$$

Since D_0 represents the kinetic energy operator, it should scale like $m_q v^2$. We can then expand the equation formally in $\frac{D_0}{m_q} \sim v^2$, introducing an infinite number of terms to eq. (2.4):

$$\frac{1}{iD_0 + 2m_q} = \frac{1}{2m_q} - \frac{iD_0}{4m_q^2} + \mathcal{O}\left(\frac{1}{m_q^3}\right)$$

To $\mathcal{O}(m_q^{-1})$, the equation of motion for ψ is

$$\left(iD_0 + \frac{(\boldsymbol{\sigma} \cdot \mathbf{D})^2}{2m_q} \right) \psi = 0 \quad (2.5)$$

³Note that $\gamma^\mu D_\mu = \gamma^0 D_0 - \boldsymbol{\gamma} \cdot \mathbf{D}$.

We can simplify the second term by writing in terms of its components

$$\begin{aligned}
\sigma^i \sigma^j D^i D^j &= \left(\frac{1}{2} \{ \sigma^i, \sigma^j \} + \frac{1}{2} [\sigma^i, \sigma^j] \right) D^i D^j \\
&= (\delta^{ij} + i\epsilon^{ijk} \sigma^k) D^i D^j \\
&= D^i D^i + \frac{1}{2} i\epsilon^{ijk} \sigma^k [D^i, D^j]
\end{aligned}$$

where we used the fact that the Levi-Civita tensor is totally antisymmetric. The commutator of covariant derivatives is related to the chromoelectric and chromomagnetic fields \mathbf{E} and \mathbf{B} as

$$E^i = i [D^0, D^i], \quad B^i = \frac{1}{2} i\epsilon^{ijk} [D^j, D^k] \quad (2.6)$$

Then our final result for the second term of eq. (2.5) is

$$\frac{(\boldsymbol{\sigma} \cdot \mathbf{D})^2}{2m_q} = \frac{\mathbf{D}^2}{2m_q} + \frac{\boldsymbol{\sigma} \cdot \mathbf{B}}{2m_q}$$

We see that the expansion in m_q^{-1} tells us that, to lowest order in v , the quark and antiquark degrees of freedom obey the Schrödinger-Pauli equation, as should be expected.

Let us now move on to the $\mathcal{O}(m_q^{-2})$ term in eq. (2.4):

$$\begin{aligned}
(i\boldsymbol{\sigma} \cdot \mathbf{D}) iD_0 (i\boldsymbol{\sigma} \cdot \mathbf{D}) &= -(i\boldsymbol{\sigma} \cdot \mathbf{D}) \sigma^j ([D_0, D^j] + D^j D_0) \\
&= -(i\boldsymbol{\sigma} \cdot \mathbf{D}) i\sigma^j E^j
\end{aligned}$$

where we used eq. (2.6) in the first term and got rid of the second term using the equations of motion eq. (2.5).⁴ Then, upon using $\sigma^i \sigma^j = \delta^{ij} + i\epsilon^{ijk} \sigma^k$ again, we have

$$(i\boldsymbol{\sigma} \cdot \mathbf{D}) iD_0 (i\boldsymbol{\sigma} \cdot \mathbf{D}) = \mathbf{D} \cdot \mathbf{E} + i\boldsymbol{\sigma} \cdot (\mathbf{D} \times \mathbf{E})$$

⁴Technically speaking, this requires a redefinition of our quark/antiquark fields; see ref. [23] for a discussion of this step in a similar context.

where the covariant derivative only acts on the chromoelectric field. However, this term is multiplied by ψ on the right, and in order to keep with our covariant derivative convention we rewrite the above as

$$(i\boldsymbol{\sigma} \cdot \mathbf{D}) iD_0 (i\boldsymbol{\sigma} \cdot \mathbf{D}) \psi = [(\mathbf{D} \cdot \mathbf{E} - \mathbf{E} \cdot \mathbf{D}) + i\boldsymbol{\sigma} \cdot (\mathbf{D} \times \mathbf{E} - \mathbf{E} \times \mathbf{D})] \psi$$

using the fact that \mathbf{D} obeys the Leibniz rule [24].

At $\mathcal{O}(m_q^{-3})$ we will only include the relativistic correction $\frac{\mathbf{D}^4}{8m_q^3}$, which will be relevant when we discuss the effects of the $\mathcal{O}(v^4)$ heavy quark propagator. Collecting all the corrections together, the bilinear part of the NRQCD Lagrangian is given by

$$\begin{aligned} \mathcal{L}_{2q} = & \psi^\dagger \left\{ iD_0 + \frac{c_1}{2m_q} \mathbf{D}^2 + \frac{c_2}{8m_q^3} \mathbf{D}^4 + \frac{c_F}{2m_q} \boldsymbol{\sigma} \cdot \mathbf{B} \right. \\ & + \frac{ic_S}{8m_q^2} \boldsymbol{\sigma} \cdot (\mathbf{D} \times \mathbf{E} - \mathbf{E} \times \mathbf{D}) + \frac{c_D}{8m_q^2} (\mathbf{D} \cdot \mathbf{E} - \mathbf{E} \cdot \mathbf{D}) + \dots \left. \right\} \psi \\ & + \left(\psi \rightarrow \chi_c, T^a \rightarrow (T^a)^T \right)^5 \end{aligned} \quad (2.7)$$

where the dynamics of the antiquark $\chi_c = -i\sigma^2 \chi^*$ is given by demanding charge conjugation symmetry, and the normalized coefficients multiplying each term are the additional dimensionless parameters of NRQCD that will be determined via matching. We see that our expansion recovered the relativistic, Fermi, spin-orbit and Darwin perturbations of non-relativistic quantum mechanics. However, as it stands this Lagrangian cannot describe the effects of annihilation on the bound state which is not desirable since, for example, the Υ meson has a nonzero decay width [24]. To account for these effects we must add local, multi-fermion interactions that create and annihilate a quark-antiquark pair in a specific spin and color state [20]

$$\mathcal{L}_{4q} = \sum_i \frac{C_F \alpha_s}{m_q^2} C_i \psi^\dagger \boldsymbol{\Gamma}_i \psi \chi_c^\dagger \boldsymbol{\Gamma}_i \chi_c \quad (2.8)$$

⁵This only applies to generators contracted with heavy quark color indices [25].

where $\mathbf{\Gamma}_i$ is a matrix in color and spin space and C_i is the corresponding matching coefficient.⁶ Then the heavy quark sector of the NRQCD Lagrangian is simply the sum of eqs. (2.7) and (2.8).

The matching coefficients are designed to take into account the (short-distance) hard scale contributions $p \sim m_q$, where asymptotic freedom allows an expansion of radiative effects in α_s . At the same time, the expansion of the NRQCD dynamics is arranged in powers of $\frac{p}{m_q} \sim v$, where in eq. (2.7) we have included all the terms necessary for $\mathcal{O}(v^4)$ accuracy. In general, when calculating a physical observable to an accuracy of $\mathcal{O}(\alpha_s^n v^m)$, one must consider all terms in the NRQCD Lagrangian up to $\mathcal{O}(v^m)$ with their coefficients computed to $\mathcal{O}(\alpha_s^n)$ accuracy.⁷

Already at this level we can perform the matching of the kinetic terms in eq. (2.7). The kinetic energy of the noninteracting quark is given by the energy-momentum relation

$$E_{\text{kin}} = \sqrt{\mathbf{p}^2 + m_q^2} - m_q = \frac{\mathbf{p}^2}{2m_q^2} - \frac{\mathbf{p}^4}{8m_q^3} + \mathcal{O}\left(\frac{\mathbf{p}^6}{m_q^5}\right)$$

Transforming to position space with the prescription $\mathbf{p} = -i\nabla$ then suggests that, in order for the energy-momentum relation to be satisfied, $c_1 = c_2 = 1$ to all orders in α_s . In other words, Poincare symmetry protects the kinetic terms from any radiative corrections [27].

2.2.1 Lattice NRQCD

As mentioned in Chapter 1, lattice simulations are one way to probe the nonperturbative sector of hadrons. This is done by the discretization of the action on a 4-dimensional Euclidean lattice, which adds two relevant length scales: the lattice spacing a and the length of the lattice “box” L . To capture the full range of heavy quarkonium dynamics, we should have the the lattice large enough to capture confinement physics at $r \sim \Lambda_{\text{QCD}}^{-1}$,

⁶When discussing the four-fermion operator responsible for hyperfine splitting in (colourless) bottomonium, that is, $\psi^\dagger \boldsymbol{\sigma} \psi \chi_c^\dagger \boldsymbol{\sigma} \chi_c$, the corresponding matching coefficient is denoted as d_σ .

⁷A common power-counting scheme is given in Table I of ref. [26].

yet fine enough to probe short-distance effects at $r \sim m_q^{-1}$. This is represented by the hierarchy

$$a \ll m_q^{-1} \ll \Lambda_{\text{QCD}}^{-1} \ll L$$

If we have a uniformly spaced lattice, then $L = Na$ where N is the number of lattice points. Remembering that the lattice simulation exists in a four-dimensional “box”, we get that the number of lattice points has the lower bound

$$N^4 \gg \left(\frac{m_q}{\Lambda_{\text{QCD}}} \right)^4 \quad (2.9)$$

which can be 25^4 for simulation of the $b\bar{b}$ system; clearly, simulating quarkonium in lattice QCD is an expensive procedure. On the other hand, the shortest dynamical scale in NRQCD is the inverse Bohr radius, which suppresses the ratio eq. (2.9) by v^4 . This allows lattice NRQCD simulations of heavy quarkonium dynamics to be within reach of realistic lattice configurations. The factorization scale μ should then be identified with the inverse lattice spacing:

$$m_q v \ll a^{-1} \ll m_q$$

This puts a constraint on the granularity of the lattice, namely that it cannot be too fine: if this constraint is not satisfied, hard modes are left dynamical resulting in a breakdown of our non-relativistic approximation. In fact, lattice NRQCD simulations are performed with spacings satisfying $am_q \gtrsim 1$, which allows a numerical polynomial fitting to obtain the continuum result for a desired observable.

Lattice NRQCD simulations require specifying the NRQCD action to $\mathcal{O}(v^n)$ accuracy, where n is a positive integer: for example, the simulations performed in ref. [7] includes all terms in the NRQCD Lagrangian up to $\mathcal{O}(v^6)$ accuracy, inclusive. The Laplacian is then discretized using a *central* difference, introducing a finite spacing error of $\mathcal{O}(a^4)$ [24]. The quark propagator is then solved for iteratively in position space, and meson properties such as the energy or wave function at the origin can then be extracted using Monte Carlo

techniques; the technical details of lattice NRQCD can be found in refs. [14, 24].

2.3 Radiative Improvement and Matching in Lattice NRQCD

For a given order in the expansion in v , NRQCD introduces a finite number of new parameters which are determined via matching. This process fixes the parameters such that, for energy scales smaller than the factorization scale, NRQCD and QCD amplitudes are equal. This is usually done perturbatively by the following recipe [20]:

1. Use perturbative QCD to calculate scattering amplitudes between asymptotic quark and gluon states to a given order in α_s and expand them in powers of v .
2. Use perturbative NRQCD to compute the same scattering amplitudes to the same order in α_s and v .
3. Tune the NRQCD parameters so that the two results are equal order-by-order in α_s and v .

Let us apply this recipe to the matching for the NRQCD four-fermion operators, done by computing the one-particle irreducible (1PI) diagrams of $q\bar{q} \rightarrow q\bar{q}$ transitions in QCD and NRQCD. In particular, the matching between the spin-dependent part of the ladder diagrams can be represented diagrammatically as

$$\text{QCD Ladder} = \frac{d_\sigma}{m_q^2} \text{Contact Term} + \text{NRQCD Ladder} + \dots$$

where the LHS is given by the QCD Feynman rules (see ref. [11]) and the RHS is given by the NRQCD Feynman rules in Appendix A. However, we will see in Chapter 3 that when performing the matching for lattice NRQCD with the factorization cutoff $\mu \sim a^{-1}$, we

should not match scattering amplitudes of free quarks and antiquarks but instead match bound state amplitudes of the NRQCD four-fermion operators. This is due to the fact that, for the specific case of lattice regularization, an expansion in α_s and an expansion in a do not commute and one must account for all-order Coulomb exchanges *before* taking the $a \rightarrow 0$ limit. This subtle point is the central claim of this thesis and we will show in Chapter 4 that this is the cause of the discrepancy between the results of refs. [3, 7] for the ground state hyperfine splitting in the $b\bar{b}$ system. To describe this effect in NRQCD to $\mathcal{O}(v^4)$, we need to look at the spin-dependent portion of the NRQCD Lagrangian:

$$\mathcal{L}_\sigma = c_F \psi^\dagger \frac{\boldsymbol{\sigma} \cdot \mathbf{B}}{2m_q} \psi + (\psi \rightarrow \chi_c) + d_\sigma \frac{C_F \alpha_s}{m_q^2} \psi^\dagger \boldsymbol{\sigma} \psi \chi_c^\dagger \boldsymbol{\sigma} \chi_c$$

where the spin-orbit coupling proportional to c_S is neglected since we are considering $l = 0$ S-waves, and the four-fermion interaction is projected onto the color-singlet since we are considering a colorless meson. Until recently, lattice NRQCD simulations have used the tree-level values for the matching coefficients, namely that $c_F = 1$, $d_\sigma = 0$. However, radiative corrections to c_F and d_σ , as well as the inclusion of spin-dependent $\mathcal{O}(v^6)$ terms, could reduce the systematic error by around 6 MeV [7]. Therefore, the radiative improvement of the lattice NRQCD action is vital for a precise determination of the bottomonium $1S$ hyperfine splitting.

Let us now focus on the spin-dependent four-fermion matching coefficient d_σ . To perform the matching, we need to consider the 1PI quark-antiquark scattering amplitudes in QCD, which is given by (to 1-loop)

$$\mathcal{M}_{1\text{PI}}^{\text{QCD}} = \frac{C_F \alpha_s^2}{m_q^2} \left[\frac{C_A}{2} \ln \left(\frac{m_q}{\lambda} \right) + T_F (\ln 2 - 1) + C_F \left(1 - \frac{2\pi m_q}{3\lambda} \right) \right] \psi^\dagger \boldsymbol{\sigma} \psi \chi_c^\dagger \boldsymbol{\sigma} \chi_c \quad (2.10)$$

where $T_F = \frac{1}{2}$, $C_F = \frac{N_c^2 - 1}{2N}$, $C_A = N_c$ are colour factors for $SU(N_c)$, and λ is a fictitious gluon mass introduced to regulate the IR divergence in the ladder diagrams pictured above [3]. To complete the matching, we need to compute the spin-dependent 1PI diagrams in

lattice NRQCD. Below we outline the two ways this can be performed.

2.3.1 Expansion About the Continuum Limit

This method is explained in full detail in ref. [3] and is based on the asymptotic expansion of the lattice loop integrals about the continuum limit, allowing a systematic expansion in the lattice spacing a [28]. To the same order in m_q^{-1} as eq. (2.10), the 1PI lattice NRQCD amplitude is

$$\mathcal{M}_{1\text{PI}}^{\text{NRQCD}} = \frac{C_F \alpha_s^2}{m_q^2} \left[- \left(\delta + \frac{1}{2} \ln(a\lambda) \right) C_A - \frac{2\pi m_q}{3\lambda} C_F + \frac{d_\sigma}{\alpha_s} \right] \psi^\dagger \boldsymbol{\sigma} \psi \chi_c^\dagger \boldsymbol{\sigma} \chi_c + \mathcal{O}(a) \quad (2.11)$$

where δ is the non-logarithmic contribution from the non-abelian diagrams which depends on a particular realization of the lattice action [3]. The $\mathcal{O}(a)$ term in particular arises from the ladder diagrams in lattice NRQCD, and is ignored as we eventually take the $a \rightarrow 0$ limit. Then to leading order in a and m_q^{-1} , the four-fermion matching coefficient is given by

$$d_\sigma = \alpha_s \left[\left(\delta + \frac{L}{2} \right) C_A + (\ln 2 - 1) T_F + C_F \right]$$

where $L = \ln(am_q)$. The main problem is then the determination of δ , which is done in a semi-analytic approach; the details can be explored in ref. [3]. For the HPQCD action in ref. [6], the final result is

$$\delta = 0.1446(28)$$

Note that this method gives a matching coefficient that depends only logarithmically on the lattice spacing to this order in m_q^{-1} . Therefore, we avoid issues with the ill-defined continuum limit of lattice NRQCD. If we were to include the higher-order terms of the NRQCD Lagrangian, the matching coefficient would include the divergent positive powers of $(am_q)^{-1}$ [1]. In any case, these terms are suppressed since lattice NRQCD simulations are performed for coarse lattice spacings $a \gg m_q^{-1}$.

2.3.2 Direct Numerical Matching

Perturbative matching has been the traditional method used for the radiative improvement of the lattice NRQCD action and is the method implemented in NRQCD simulations to incorporate the four-fermion improvement [4,5]. For the four-fermion operator, the logarithmic and annihilation contributions to the 1PI diagram are given analytically while the other contributions including the ladder diagrams are computed numerically and depend on the combination am_q . The matching coefficient can then be written as ⁸

$$d_\sigma = \alpha_s \left[\frac{L}{2} C_A + (\ln 2 - 1) T_F + D(am_q) \right]$$

where the function $D(am_q)$ can formally be expanded in the asymptotic series

$$D(am_q) = \sum_{n=n_0}^{\infty} (am_q)^n \Delta^{(n)} \quad (2.12)$$

where $n_0 < 0$; $D(am_q)$ carries the non-logarithmic dependence on the lattice spacing. For $am_q > 1$ we can ignore terms in eq. (2.12) with $n < 0$ and fit the numerical results to obtain the coefficients of the expansion eq. (2.12) [7]. The lattice spacings used in the $\mathcal{O}(v^4)$ action in ref. [5] are $am_q = 1.95, 2.8$, and 4.0 and performing a linear fit of the coefficients gives

$$\Delta^{(0)} = 3.66(4), \quad \Delta^{(1)} = -1.81(9) \quad (2.13)$$

Meanwhile the lattice spacings used in the $\mathcal{O}(v^6)$ action [7] are $am_q = 1.95, 2.73$, and 3.31 and a similar fitting gives

$$\Delta^{(0)} = 1.31(3), \quad \Delta^{(1)} = -1.52(1) \quad (2.14)$$

⁸In this thesis, $\frac{d_\sigma}{\alpha_s}$ should be compared with $\frac{9}{8}(d_1 - d_2)$ in refs. [4–7].

Note that higher order fits cannot be performed due to the lack of sufficient numerical values for am_q , so that the uncertainty may be larger than what we indicate in the parenthesis. We can compare our zeroth order term to the Wilson coefficient obtained from the previous subsection

$$\Delta^{(0)} = C_A\delta + C_F = 1.767(9)$$

which roughly agrees with the $\mathcal{O}(v^6)$ action, and with better agreement expected when higher-order terms in the velocity expansion are included.

Note that while the expansion about the continuum limit does not determine the terms dependent on positive powers of the lattice spacing, the standard matching differs in that it retains this dependence in the Wilson coefficient. The actual dependence of the Wilson coefficients on a is discussed in the next chapter.

Chapter 3

Coulomb Binding Effects on the Lattice

3.1 Coulomb Binding Effects

The binding effects within a Coulomb bound state are dominated by the *potential region* of scales. In this region, the quark and antiquark fields ψ and χ_c respectively are *on-shell*, meaning that they obey their equations of motion given by, to lowest order,

$$\left(iD_0 + \frac{\mathbf{D}^2}{2m_q}\right)\psi = 0, \quad \left(iD_0 - \frac{\mathbf{D}^2}{2m_q}\right)\chi_c = 0 \quad (3.1)$$

Forgetting about strong interactions momentarily, eq. (3.1) in momentum space is given by

$$\left(q_0 - \frac{\mathbf{q}^2}{2m_q}\right)\psi = 0, \quad \left(q_0 + \frac{\mathbf{q}^2}{2m_q}\right)\chi_c = 0 \quad (3.2)$$

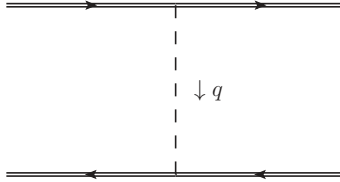
where q_0 and \mathbf{q} are the energy and momentum transfer respectively. A bound state's characteristic length scale is given by its Bohr radius r_b , which scales as $(m_q v)^{-1}$. This

then implies that in the potential region,

$$q_0 \sim m_q v^2, \quad |\mathbf{q}| \sim m_q v$$

since the momentum transfer scales roughly as the inverse Bohr radius.

In a general quantum field theory, bound states appear as poles in the scattering amplitude of the constituent degrees of freedom [29]. This occurs precisely when the perturbative expansion in the coupling constant is singular, and one has to resum all the contributions via the Bethe-Salpeter equation. Thus, we can explore the Coulomb binding effects in bound states by finding the set of diagrams that contribute to all orders in α_s in the potential region. We claim that n -loop planar Coulomb exchanges are the only diagrams that are singular in this way. At leading order ($n = 0$), this looks like



where $q^\mu \equiv (q_0, \mathbf{q})$ is the energy and momentum transfer of the virtual Coulomb gluon. Using the NRQCD Feynman rules in Appendix A and projecting to the color-singlet state, we can assign a factor $C_F \alpha_s$ to the two vertices. Also since in the potential region we have

$$\frac{1}{q^2} = \frac{1}{q_0^2 - \mathbf{q}^2} \sim \frac{1}{(m_q v)^2}$$

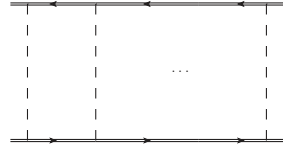
the tree-level diagram can be estimated to be

$$\begin{array}{c} \text{---} \rightarrow \text{---} \\ | \\ \text{---} \leftarrow \text{---} \end{array} \quad \downarrow q \quad \sim \frac{1}{m_q^2 v} \left(\frac{\alpha_s}{v} \right) \quad (3.3)$$

Let us now investigate the analogous ladder diagrams at n -loops. We have

- α_s^{n+1} from vertices
- $(m_q v)^{-2(n+1)}$ from gluon propagators
- $(m_q v^2)^{(-2n)}$ from the quark/antiquark propagators
- $(m_q v^2)^n (m_q v)^n$ from the integration measures $(dq_0 d^3\mathbf{q})^n$

combining these factors together, we have that the n -loop diagram is given by



$$\sim \frac{1}{m_q^2 v} \left(\frac{\alpha_s}{v} \right)^{n+1} \quad (3.4)$$

Let us now consider the heavy quark limit, where the potential energy between the quark and antiquark is dominated by the Coulomb potential and confinement effects are suppressed. The size of the bound state is determined by a balance in the kinetic and potential energies

$$m_q v^2 \sim \frac{\alpha_s}{r}$$

where r is the separation between the quark and antiquark. However since $r_b \sim (m_q v)^{-1}$ is the characteristic length scale of the bound state, we have that

$$v \sim \alpha_s$$

Thus, the n -loop ladder contribution in eq. (3.4) is of the same size as the tree-level amplitude in eq. (3.3), and such diagrams must be resummed to all orders by the Bethe-Salpeter integral equation, with the kernel representing a tree-level ladder exchange. Fortunately, this is exactly equivalent to solving the Schrödinger equation with the Coulomb potential $V(r) = -C_F \alpha_s / r$ for the bound state wave function Ψ [30]. In position space this is given by

$$\left(E + \frac{\nabla^2}{m_q} \right) \Psi(r) = V(r) \Psi(r) \quad (3.5)$$

where $E < 0$ is the energy of the bound state. With $\nabla^2 \rightarrow -\mathbf{p}^2$ as well as the fact that pointwise multiplication in a given vector space leads to a convolution in its Fourier conjugate space, we can write eq. (3.5) in momentum space as

$$\tilde{\Psi}(p) = \frac{1}{\frac{\mathbf{p}^2}{m_q} - E} \int \frac{d^3k}{(2\pi)^3} \frac{4\pi C_F \alpha_s}{|\mathbf{p} - \mathbf{k}|^2} \tilde{\Psi}(k) \quad (3.6)$$

where

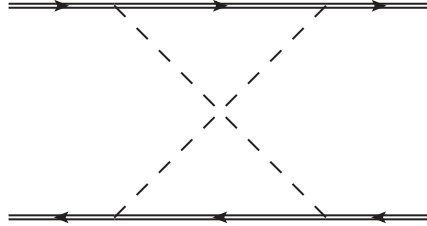
$$\tilde{\Psi}(p) = \int d^3x \Psi(x) e^{-i\mathbf{p}\cdot\mathbf{x}} \quad (3.7)$$

The Schrödinger equation can be represented diagrammatically as



We see that Coulomb binding effects are nonperturbative in α_s and can only be taken into account by solving for the bound state wave function.

The astute reader will note that the non-planar (crossed) ladder diagrams



scale the same way as the planar ladder diagrams. To all orders, these diagrams do not contribute to the scattering amplitude in the potential region. The reason is that the poles of the quark propagators in the complex energy plane are on the same imaginary half-plane, so that one can close the contour without picking up any residues. As a result, the diagram gives 0 in the potential region.

In the leading Coulomb approximation, the only scale in NRQCD is $m_q \alpha_s$. Therefore,

as the n -loop planar Coulomb exchanges are UV-finite, the lattice regularization results in terms proportional to powers of $am_q\alpha_s$, which vanish in the continuum limit: such terms are called *Coulomb lattice artifacts*. As physical results for observables should be independent of a , a proper account of the lattice spacing dependence is crucial to obtaining the correct continuum value. Let us now investigate two methods of obtaining the Coulomb lattice artifacts, namely comparing the 1-loop Coulomb exchange and the all-order approach based on the Schrödinger equation.

3.2 Coulomb Artifact to 1-Loop

The $\mathcal{O}(v^4)$ spin-dependent lattice NRQCD planar ladder diagram is given by only one diagram at one-loop:

$$i\mathcal{M} = 2 \times \begin{array}{c} \text{---} \bullet \text{---} \\ | \text{wavy} \\ \text{---} \bullet \text{---} \end{array} \quad (3.8)$$

where the black dots represent the spin-flip operator proportional to $c_F = 1 + \mathcal{O}(\alpha_s)$ and the factor of 2 comes from the two different ways we can order the gluon exchanges. We will compute this diagram on a spherical lattice, where only the radial axis is discretized and the lattice spacing serves as a UV cutoff at $\Lambda_{\text{UV}} = \pi/a$. Note that since the lattice heavy quark and gluon propagators only generate terms of $\mathcal{O}(a^2)$, and we are only interested in obtaining the linear dependence on a , we can use the continuum NRQCD propagators given in Appendix A [28]. The details of the calculation are included in Appendix B.2, and the amplitude is

$$\mathcal{M} = \frac{C_F\alpha_s^2}{m_q^2} \left[-\frac{2\pi m_q}{3\lambda} C_F + \frac{16C_F}{3\pi} am_q \right] + \mathcal{O}(a^3) \quad (3.9)$$

We see that the zeroth order term in a reproduces the IR contribution in the QCD amplitude eq. (2.10). We can now use the four-fermion matching mentioned in Section

2.3 to determine the value of the Coulomb exchange to the matching coefficient d_σ :

$$\frac{C_F \alpha_s^2}{m_q^2} \left[0 - \left(\frac{16 C_F}{3\pi} a m_q \right) \right] \psi^\dagger \boldsymbol{\sigma} \psi \chi_c^\dagger \boldsymbol{\sigma} \chi_c = d_\sigma \frac{C_F \alpha_s}{m_q^2} \psi^\dagger \boldsymbol{\sigma} \psi \chi_c^\dagger \boldsymbol{\sigma} \chi_c$$

where the first term in eq. (3.9) is 0 since lattice NRQCD and continuum QCD share the same IR behaviour by definition. When comparing with the expansion eq. (2.12), we have that the coefficient of the linear lattice artifact due to the 1-loop Coulomb exchange is

$$\Delta^{(1)} = -\nu \frac{16}{3\pi} C_F \approx -1.88 \quad (3.10)$$

where $\nu = 0.831 \dots$ is a geometrical factor that converts our result to the one obtained with a cubic lattice [3]. Including this factor allows us to compare our value eq. (3.10) to the real lattice results given in eqs. (2.13) and (2.14) which are $\Delta^{(1)} = -1.82$ and -1.52 for the $\mathcal{O}(v^4)$ and $\mathcal{O}(v^6)$ actions, respectively. We see that our estimation of the one-loop Coulomb pinch is in good agreement with the real linear lattice artifacts, and due to its relatively large value, this term dominates the expansion in eq. (2.12).

3.3 Coulomb Artifact to All Orders

In the last subsection, to study the Coulomb lattice artifacts, we performed the matching between scattering amplitudes of free quarks and antiquarks. We can try to account for Coulomb artifacts without an expansion in the strong coupling constant by considering *not* scattering amplitudes with free quark and antiquark external states, but amplitudes with the external quarkonium bound state instead. As a result, we can absorb the Coulomb exchange in the 1-loop diagram using the Schrödinger equation:



On the lattice, this means that all Coulomb lattice artifacts are embedded in the wave function, so that the matching procedure is performed by averaging the NRQCD four-fermion operators with wave functions computed in the lattice and the continuum. These averages are proportional to the wave function at the origin since the four-fermion operators are local, ie. proportional to $\delta^3(\mathbf{r})$. We refer to this modified matching procedure by the name of “Schrödinger matching.” The corresponding correction to the energy levels is then proportional to

$$\left(1 - \frac{|\Psi_l(0)|^2}{|\Psi_c(0)|^2}\right) \langle O_i \rangle \quad (3.11)$$

where $\Psi(0)$ is the wave function at the origin with the subscript distinguishing whether it is computed on the lattice or the continuum, and O_i is the NRQCD four-fermion operator in consideration (see eq. (2.8)). We should emphasize that eq. (3.11) includes all-order dependence on the strong coupling constant via the combination $am_q\alpha_s$.

Let’s apply this method to the four-fermion spin-dependent matching coefficient d_σ . The spin-dependent tree-level diagram is calculated in Appendix B.1 as

$$\mathcal{M} = -\frac{2\pi}{3} \frac{C_F\alpha_s}{m_q^2} \psi^\dagger \boldsymbol{\sigma} \psi \chi_c^\dagger \boldsymbol{\sigma} \chi_c$$

which is constant in the momentum transfer within the potential region. The continuum wave function is solved for in Appendix C and is given by $\Psi_c(r) = \frac{1}{\sqrt{\pi}} e^{-r}$ in Coulomb units, where the unit of length is the Bohr radius $r_b = 2/C_F\alpha_s m_q$.¹ To implement the Schrödinger matching, we now must find the lattice wave function at the origin.

In the formal limit $\Lambda_{\text{QCD}} \lesssim m_q v^2$, solving the discretized Schrödinger equation for the lattice wave function reproduces the real bound state wave function obtained in lattice NRQCD simulations. Our approach, detailed in Appendix C, is to solve the Schrödinger equation on a spherical lattice obtained by the discretization of the radial axis only, with $r_n = na$ for $n = 0, 1, \dots$. In this case, the angular part is still given by the zeroth-order

¹We will now switch from natural to Coulomb units until we explicitly state otherwise.

spherical harmonic $Y_0^0 = \frac{1}{\sqrt{4\pi}}$. The lattice radial solution $u(n) = \sqrt{4\pi} na \Psi_l(n)$ is found by replacing the radial part of the Laplacian in eq. (3.5) with a central difference, resulting in the radial equation

$$u(n+1) - 2u(n) + u(n-1) + 2a^2 \left(\frac{1}{na} + E_l \right) u(n) = 0 \quad (3.12)$$

where $n = 1, 2, \dots$, the boundary condition is $u(0) = 0$, and E_l is the lattice binding energy. Note that the central difference, chosen to replicate what is done in real lattice simulations, results in $\mathcal{O}(a^2)$ local error in the lattice wave function [24]. Now that we have a difference equation, we can pursue a solution numerically via the “shooting method” method explained in ref. [31] to search for the correct energy eigenvalue, along with the radial equation (3.12) to build the wave function all the way to the origin $n = 0$. This approach is detailed in Appendix C and allows us to obtain the lattice spacing dependence reliably to $\mathcal{O}(a^4)$ [1]. Another approach is to solve the difference equation *analytically* using the exact ground state solution of the Coulomb problem on a one-dimensional lattice [2, 32]. The lattice wave function and its associated ground state energy, to *all* orders in a , is then

$$\begin{aligned} \Psi_l(n) &= \frac{1}{\sqrt{\pi}} \frac{1}{(1+a^2)^{1/4}} \exp(-n \operatorname{arcsinh} a) = \Psi_c(r) + \mathcal{O}(a^2) \\ E_l &= -\frac{1}{a^2} \left[(1+a^2)^{1/2} - 1 \right] = E_c + \mathcal{O}(a^2) \end{aligned} \quad (3.13)$$

where $E_c = -\frac{1}{2}$ is the binding energy of the quark-antiquark pair in the continuum. The wave function satisfies the normalization condition

$$4\pi a^3 \sum_{n=0}^{\infty} n^2 |\Psi_l(n)|^2 = 1$$

Note that a characteristic feature of eq. (3.13) is the absence of a linear term in a , in disagreement with the one-loop result eq. (3.10). This is completely independent of the

particular lattice geometry chosen; a study of the Schrödinger-Pauli equation on a cubic lattice performed in ref. [33] also demonstrated that Coulomb effects do not generate a linear artifact. Instead, the fact there are no odd powers on the lattice spacing results from using a central difference discretization for the Laplacian (see Theorem 8.10 in ref. [34]). We discuss the differences between the one-loop and all-order approaches in the next section.

3.4 Breakdown of Perturbative Matching

Since the UV cutoff is a short-distance effect, one may think that the lattice dependence should be accountable within the perturbative matching procedure. Thus one may expect that the expansion of eq. (3.11) should give rise to the one-loop linear lattice artifact with coefficient given by eq. (3.10). However, in this section we are going to show that the effects of space discretization on the Coulomb dynamics cannot be accounted for order by order in α_s and require the exact solution of the Coulomb problem without the expansion in the strong coupling constant. To investigate the difference between the two methods, and because perturbative matching is performed in momentum space, we must consider the lattice momentum wave function as defined by the Fourier transform

$$\begin{aligned}\tilde{\Psi}_l(p) &= 4\pi a^3 \sum_{n=0}^{\infty} n^2 \Psi_l(n) \frac{\sin(npa)}{npa} \\ &= \frac{8\sqrt{\pi}}{(1+a^2)^{1/4}} \frac{(a/2)^4}{(\sin^2(pa/2) - a^2 E_l/2)^2} \frac{\sin(pa)}{pa} \\ &= \tilde{\Psi}_c(p) + \mathcal{O}(a^2)\end{aligned}\tag{3.14}$$

where $\tilde{\Psi}_c(p) = \frac{8\sqrt{\pi}}{(p^2+1)^2}$ is the continuum wave function in momentum space. Interestingly enough the spatial wave function at the origin, $\Psi_l(n=0)$, does not contribute to the lattice momentum wave function because of the n^2 factor: the sum in eq. (3.14) begins

with $n = 1$. The inverse Fourier transform, given by

$$\Psi_l(n) = \frac{1}{2\pi^2} \int_0^{\frac{\pi}{a}} dp p^2 \tilde{\Psi}_l(p) \frac{\sin(npa)}{npa} \quad (3.15)$$

then only holds for lattice sites $n \neq 0$. Indeed, the corresponding integral for $n = 0$ gives²

$$\begin{aligned} \Psi_p(0) &\equiv \frac{1}{2\pi^2} \int_0^{\frac{\pi}{a}} dp p^2 \tilde{\Psi}_l(p) \\ &= \frac{1}{\sqrt{\pi}} \left(1 - \frac{\sqrt{1+a^2} - 1}{a} \right) = \Psi_c(0) \left[1 - \frac{a}{2} + \mathcal{O}(a^2) \right] \end{aligned} \quad (3.16)$$

while the spatial wave function at the origin is given by

$$\Psi_l(0) = \frac{1}{\sqrt{\pi}} \frac{1}{(1+a^2)^{1/4}} = \Psi_c(0) \left[1 - \frac{a^2}{4} + \mathcal{O}(a^2) \right]$$

While both functions have the same continuum limit, one function satisfies the Schrödinger equation while the other does not. To show this let us consider the forward derivative of the two functions at the origin. For the solution eq. (3.13), we have

$$\Psi_l'(0) = \frac{\Psi_l(1) - \Psi_l(0)}{a} = -\Psi_c(0) + \mathcal{O}(a)$$

which, in the limit $a \rightarrow 0$, recovers the property of the continuum solution:

$$\Psi_c'(0) = -\frac{1}{\sqrt{\pi}} e^{-r} \Big|_{r=0} = -\Psi_c(0) \quad (3.17)$$

Now, if instead we use the inverse Fourier transform result eq. (3.16), we get

$$\Psi_l'(0) = \frac{\Psi_l(1) - \Psi_p(0)}{a} = -\frac{1}{2} \Psi_c(0) + \mathcal{O}(a)$$

²The subscript p in eq. (3.16) is used to distinguish the result from the inverse Fourier transform from the value of the solution given in eq. (3.13).

which violates the continuum result at $\mathcal{O}(1)$ [2].

We should note that while the linear term in eq. (3.16) is universal for all the S-wave states, the coefficient of the quadratic terms in the expansion of the bound state parameters in a is sensitive to the Coulomb dynamics, e.g. for the first excited state this coefficient in eq. (3.4) changes from $-1/4$ to $1/16$.

We now demonstrate that the nonvanishing $\mathcal{O}(a)$ term in eq. (3.16) is the origin of the linear artifact discussed in Section 3.2. The non-relativistic Coulomb dynamics is not sensitive to the high momentum region and, to the leading order in v , the result for such a contribution obtained within continuum QCD and NRQCD coincide. Thus, in the standard perturbative matching, the contribution to d_σ from the Coulomb exchange comes from the difference between continuum and lattice NRQCD one-loop expressions, which, when the quarks are at rest and on threshold, is given by,

$$\delta d_\sigma = \frac{4C_F\alpha_s}{\pi} \left(\int_\lambda^\infty dp p^2 D_c(p) G_c(p) - \int_\lambda^{\frac{\pi}{a}} dp p^2 D_l(p) G_l(p) \right) \quad (3.18)$$

where the integration over the time component of the was performed by taking the residue of the heavy quark propagator, an IR cutoff λ is introduced, and we switch back to natural units. The continuum Coulomb gluon and heavy quark propagators are given by

$$D_c(p) = \frac{1}{p^2}, \quad G_c(p) = \frac{m_q}{p^2}$$

and correspond to the $\mathcal{O}(v^2)$ NRQCD action. The lattice versions are given by

$$D_l(p) = \frac{\sin(ap)}{ap} \frac{(a/2)^2}{\sin^2(ap/2)}, \quad G_l(p) = \frac{m_q(a/2)^2}{\sin^2(ap/2)}$$

After integration we get

$$\delta d_\sigma = \frac{1}{2} C_F \alpha_s a m_q + \mathcal{O}((\lambda a)^2) \quad (3.19)$$

The main effect of the lattice regularization comes from the UV cutoff at $p \sim a^{-1}$: indeed

if the continuum propagators are used in the second term of eq. (3.18), the coefficient in eq. (3.19) is changed only from $1/2$ to $4/\pi^2 = 0.405\dots$ [2].

The lattice contribution to eq. (3.18) can be obtained by the expansion of the lattice momentum wave function $\tilde{\Psi}_l(p)$ in eq. (3.16) to the first order in α_s .³ Hence, as one may expect from the general arguments, eq. (3.19) agrees with the expansion of the first factor in eq. (3.11) to the first order in α_s if the momentum space result eq. (3.16) is used to define the value of the wave function at the origin. However eq. (3.16) does not agree with the actual solution eq. (3.4) and results in a pathological wave function which does not satisfy the Schrödinger equation in the continuum limit at $r = 0$. Thus the Wilson coefficient eq. (3.19) *does not* cancel the dependence of the $\mathcal{O}(v^4)$ tree gluon exchange matrix element on a and we observe a breakdown of perturbative matching in the analysis of the Coulomb artifacts already in one loop. By contrast the Schrödinger matching with the exact solution of the Coulomb problem on the lattice gives the correct result for the Coulomb artifacts to all orders in α_s [2].

We can trace the origin of this phenomenon to the fact that the relation eq. (3.17), violated by eqs. (3.16) and (3.19), follows from the cancellation of the singular kinetic and potential energy terms in the Schrödinger equation at $r \rightarrow 0$. Indeed in the continuum the radial equation for the S-wave function is given by

$$\left(\frac{d^2}{dr^2} + \frac{2}{r} \frac{d}{dr} + \frac{C_F \alpha_s m_q}{r} + m_q E \right) \Psi(r) = 0 \quad (3.20)$$

Keeping the most singular terms in the limit $r \rightarrow 0$ we get

$$\left. \frac{d\Psi(r)}{dr} \right|_{r=0} = -\frac{1}{r_B} \Psi(r) \Big|_{r=0} \quad (3.21)$$

which reproduces eq. (3.17) in natural units. The LHS (RHS) term in the above equation correspond to the kinetic (potential) energy contribution. Hence at the origin these

³In Coulomb units, this can be done by expanding in a but keeping the combination ap fixed.

terms should be considered on an equal footing while the standard matching treats the Coulomb potential as a perturbation. Evidently the above mechanism of the perturbative matching breakdown is specific to the lattice regularization and the contact interaction in the NRQCD Lagrangian.

We can regularize the contact interaction by separating the quark and antiquark fields with a small spatial interval $r_0 \sim a$ and take the limit $r_0 \rightarrow 0$ after the matching is done. This introduces an additional $\sin(r_0 p)/r_0 p$ factor into the integrands of eq. (3.18) (see eq. (3.15)). The lattice integral then reads

$$m_q \int_{\lambda}^{\frac{\pi}{a}} dp p^2 \frac{\sin(r_0 p)}{r_0 p} \frac{\sin(ap)}{ap} \left(\frac{a/2}{\sin(ap/2)} \right)^4 = m_q \left(\frac{1}{\lambda} - \frac{\pi}{4} r_0 \right) + \mathcal{O}((\lambda a)^2) \quad (3.22)$$

which removes the $\mathcal{O}(a)$ contribution from the Wilson coefficient eq. (3.19) and brings it into agreement with the Schrödinger matching result.

We should emphasize the difference between matching calculations in lattice NRQCD and in continuum NRQCD with an explicit momentum cutoff $\Lambda_{UV} \sim a^{-1}$, which is not plagued by the problem discussed above. In the latter theory the properties of the solution of the Coulomb problem in the (continuum) coordinate space are significantly different from the solution of the finite difference equation eq. (3.12). The Schrödinger equation in this case is a differential equation and its regular solution satisfies the conditions of the Fourier inversion theorem. Hence the value of the wave function at the origin is unambiguously determined by the integral of the wave function in momentum space and the problem discussed in the previous section does not exist. The correct behaviour of the wave function and its derivative at $r \rightarrow 0$ then follows from the continuity and smoothness of the solution.

A comprehensive analysis of the four-fermion operator matching with an explicit momentum cutoff can be found in ref. [35] in the context of the NRQED calculation of the radiative corrections to the orthopositronium decay rate. In ref. [35] a numerical solution

of the coordinate-space Schrödinger equation has been obtained for the Hamiltonian defined in a momentum cutoff regularization scheme. It has been found that the dependence of the value of the resulting wave function at the origin on the cutoff includes a linear Coulomb artifacts which is cancelled by the $O(\alpha_s m_q/\Lambda_{\text{UV}})$ term in the one-loop Wilson coefficient. Thus in the momentum cutoff scheme the results of the perturbative and Schrödinger matching do agree.

Chapter 4

Determination of the Energy

Spectrum From the Lattice Data

Let us now consider how the analysis in the previous chapter affects the determination of the bottomonium spectrum in the radiatively improved lattice NRQCD. The results of nonperturbative lattice NRQCD simulations are typically given for $a \sim (vm_b)^{-1}$ [6,7]. The use of relatively large values of the lattice spacing ensures the suppression of the singular ultraviolet cutoff dependence from the higher order $(am_b)^{-n}$ terms, which are not removed by the finite order matching and become important at $a \sim m_b^{-1}$. At the same time it results in sizable Coulomb lattice artifacts proportional to a power of $\alpha_s am_b \sim 1$. The correct treatment of the artifacts is therefore crucial for the analysis.

In actual lattice simulations, the quarkonium bound state parameters are extracted from the asymptotic behavior of the quark-antiquark propagator at large Euclidean time. Neglecting the retardation and long-distance nonperturbative effects, which do not affect the Coulomb artifacts under consideration, this method should reproduce the properties of the solution of the Schrödinger equation for a given NRQCD Hamiltonian on the spatial lattice. As we have shown above, the perturbative matching of the four-quark operators does not correctly account for the Coulomb artifacts and, for $a \sim (vm_b)^{-1}$ and $v \sim \alpha_s$,

results in $\mathcal{O}(1)$ error in the prediction for the spectrum. For example, the one-loop matching of the spin-flip four-quark operator with the spurious linear Coulomb artifact gives the value of the bottomonium hyperfine splitting in ref. [4], which overshoots the predictions of perturbative QCD in ref. [18] by almost a factor of two, in clear conflict with the general understanding of the heavy quarkonium dynamics.

In practice the effect of the lattice artifacts is reduced by numerical extrapolation of the data to $a = 0$ [6, 7]. The extrapolation below $a \sim m_b^{-1}$ in this case is justified because for the typical values of lattice spacing the numerical effect of the $(am_b)^{-n}$ terms on the data points is small. This extrapolation effectively removes all the lattice artifacts including the $(a\Lambda_{\text{QCD}})^n$ terms associated with the effect of lattice regularization on the dynamics at the confinement scale Λ_{QCD} .¹ The problem of the perturbative matching breakdown, however, is not fully fixed by this procedure. Since the radiatively improved lattice result is supposed to be free of linear artifacts, the extrapolation is performed through a constrained fit of the data points by a polynomial in a with *vanishing* linear term. Since the bare lattice data is free of the linear Coulomb artifacts the one-loop perturbative matching in fact *introduces* a linear dependence of the radiatively improved result on a , which leads to a systematic error of the fit. At the same time the matching performed by the expansion about the continuum limit removes all the Coulomb lattice artifacts and does not have this problem [3].

Let us apply our discussion specifically to the hyperfine splitting in bottomonium. Using eq. (2.7), the four-fermion interaction corrects the energy spectrum via the perturbation

$$\delta H_{4\text{-q}} = -d_\sigma \frac{C_F \alpha_s}{m_q^2} \delta(\mathbf{x}) \boldsymbol{\sigma}_\psi \cdot \boldsymbol{\sigma}_{\chi_c}$$

where the spin matrices of the quark and antiquark are explicitly denoted. The hyperfine

¹For the bottomonium ground state this contribution is numerically suppressed with respect to the Coulomb artifacts since $\Lambda_{\text{QCD}} \ll \alpha_s m_b$.

splitting is then proportional to the spin-average

$$\langle s m | \boldsymbol{\sigma}_\psi \cdot \boldsymbol{\sigma}_{\chi_c} | s m \rangle \Big|_{s=0}^{s=1} \quad (4.1)$$

where $|s m\rangle \equiv |s_\psi m_\psi\rangle \otimes |s_{\chi_c} m_{\chi_c}\rangle$ is the bound state 2-spinor with the combined spin operator $\mathbf{S} \equiv \frac{\boldsymbol{\sigma}_\psi + \boldsymbol{\sigma}_{\chi_c}}{2}$. The average over the spins can be done by squaring this operator and using

$$\begin{aligned} S^2 |s, m\rangle &= s(s+1) |s, m\rangle \\ \left(\frac{\boldsymbol{\sigma}_i}{2}\right)^2 |s_i, m_i\rangle &= \frac{3}{4} |s_i, m_i\rangle \quad \text{for } i = \psi, \chi_c \end{aligned}$$

where the last equality holds since both quarks and antiquarks are spin-1/2. After some trivial algebra, we see that the spin average in eq. (4.1) contributes a factor of 4 to the hyperfine splitting, giving

$$\Delta E_{\text{hfs}} = -d_\sigma \frac{4C_F \alpha_s}{m_q^2} |\Psi_l(0)|^2 \quad (4.2)$$

In real lattice simulations the Laplacian is discretized using a central difference, so the bare lattice data is free of linear artifacts. The radiative improvement of the lattice action as done by the numerical perturbative matching of refs. [4, 5] then introduces a linear dependence on a by the one-loop contribution to d_σ , which leads to a systematic error when the lattice data is fitted with a vanishing linear term. The effect of this spurious contribution is quite significant, almost doubling the lattice hyperfine splitting for the most coarse lattice configuration (see Fig. 4.1). The direct matching implements the one-loop correction by multiplying the bare value with the contribution

$$\left[1 - \frac{3\alpha_s}{2\pi} \left(\frac{3}{2} \ln am_q + \frac{1}{2} (\ln 2 - 1) + D(am_q) \right) \right]$$

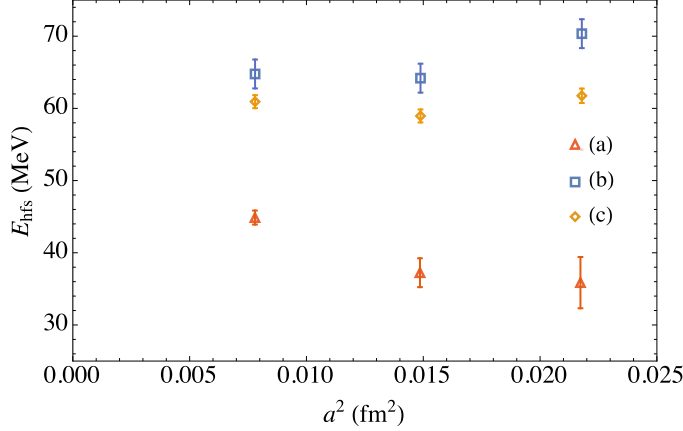


Figure 4.1: The results of the lattice simulation of the bottomonium hyperfine splitting with $\mathcal{O}(v^6)$ NRQCD action and the four-quark matching coefficient by (a) the asymptotic expansion about the continuum limit [3], (b) the direct numerical matching [5], and (c) the bare lattice result (ie. $d_\sigma = 0$) [7]. All data points include the statistical error and the uncertainty in the value of the lattice spacing. The error bars of (a) include also the uncertainty due to the higher order perturbative corrections. The difference between (a) and (b) data sets is mainly due to the spurious linear Coulomb artifact contributing to (b).

where the last term is the function defined in eq. (2.12) and has the expansion

$$D(am_q) \sim 1.31 - 1.52am_q + \mathcal{O}(a^2) \quad (4.3)$$

for the $\mathcal{O}(v^6)$ action, as discussed in Section 2.3. Extrapolating to the continuum gives a hyperfine splitting of $E_{\text{hfs}} = 60.0 \pm 6.4$ MeV. However, if the linear term in eq. (4.3) is not included in the correction, the extrapolation gives a central value of $E_{\text{hfs}} = 52.7$ MeV. This is in very good agreement with the result based on the asymptotic expansion about the continuum limit for the $\mathcal{O}(v^6)$ action, which gives a value of $E_{\text{hfs}} = 51.5 \pm 5.7$ MeV. Yet the discrepancy between the results of refs. [7] and [3] is beyond the discretization/extrapolation uncertainty, which is below 3 MeV. Thus the analysis of the hyperfine splitting in refs. [4–7] contains a systematic error and should be corrected [1]. At the same time the perturbative matching can be used for the self-consistent analysis of the quarkonium spectrum within the above extrapolation scheme if the Coulomb artifacts are

removed from the Wilson coefficients by means of the asymptotic expansion (as in ref. [3]) or a numerical fit (as in ref. [1]).

We can also estimate the lattice dependence on the quadratic Coulomb artifacts using our result for the wave function at the origin eq. (3.4):

$$E_{\text{hfs}}^{\text{lattice}} = E_{\text{hfs}} \left[1 - (\Lambda a)^2 + \mathcal{O}(a^4) \right], \quad \Lambda = \frac{C_F \alpha_s m_q}{2\sqrt{2}} \sim 530 \text{ MeV} \quad (4.4)$$

where the values for the quark mass and strong coupling constant are taken in the middle of a typical interval for the lattice spacing [1]. Meanwhile the result in ref. [3] gives $\Lambda \sim 360$ MeV for the $\mathcal{O}(v^4)$ action and $\Lambda \sim 790$ MeV for the $\mathcal{O}(v^6)$ action, in good agreement with eq. (4.4). We see that the effect of lattice artifacts is enhanced when considering the higher dimension operators as they are more sensitive to the UV momentum region.² Thus while the errors due to relativistic corrections are smaller for the $\mathcal{O}(v^6)$ action, there is a compensating larger discretization error than the one for the $\mathcal{O}(v^4)$ action. The best estimate is simply the weighted sum of the two results, giving

$$E_{\text{hfs}} = 52.9 \pm 5.5 \text{ MeV} \quad (4.5)$$

This is an unambiguous result and it is also the most accurate lattice NRQCD prediction for the $1S$ hyperfine splitting in bottomonium so far.

4.1 Summary

In this thesis we examined the matching procedure for lattice NRQCD for the radiative improvement of the four-fermion operators. We have demonstrated that binding effects are responsible for a breakdown of perturbative matching for terms that disappear in the continuum limit. This is solved by using the Schrödinger matching, which gives the correct

²This is demonstrated in Appendix B, where including the relativistic correction to the quark propagator doubles the one-loop result for the lattice artifact.

dependence on the lattice spacing. We applied our analysis to the hyperfine splitting of the bottomonium system, and resolved the discrepancy between the two latest lattice NRQCD predictions in refs. [3, 7] in favor of the result of ref. [3], which is in excellent agreement with the most precise experimental value from the Belle collaboration [19].

It is interesting to compare this result with another lattice simulation, this time based on lattice QCD. While the large window between the bottom quark and QCD scale (see Section 2.2.1) makes lattice QCD simulations of bottomonium physics quite costly, one can nevertheless make a prediction of the hyperfine splitting by extrapolating the lighter quarkonium spectrum to the physical value of the bottom quark mass [36]. This gives 53 ± 5 MeV, in very good agreement with the lattice NRQCD result eq. (4.5). Both are in good agreement with the phenomenological result based on perturbative QCD 41 ± 14 MeV [18].

Further measurements by the Babar and CLEO collaborations (refs. [37, 38] respectively) push the PDG average to 62.3 ± 3.2 MeV, which is still beyond both the lattice and phenomenological results mentioned above [15]. Further high-precision studies of the $\eta_b(1S)$ mass would be desirable to clear up the discrepancies amongst experimental groups.

We should note that the matching method we have constructed is not specific to the four-fermion term responsible for the hyperfine splitting. Indeed it is a general procedure that can be used to obtain the terms vanishing in the continuum limit for the spin-independent four-fermion matching coefficients as well. However, these coefficients are much more difficult to compute and do not presently exist in the literature [5]. A consistent treatment of the matching of these coefficients would be possible within the Schrödinger framework that we suggest.

Bibliography

- [1] T. Liu, A. A. Penin and A. Rayyan, JHEP **1702**, 084 (2017).
- [2] A. Penin and A. Rayyan, JHEP **1712**, 007 (2017).
- [3] M. Baker, A. A. Penin, D. Seidel and N. Zerf, Phys. Rev. D **92**, 054502 (2015).
- [4] T. C. Hammant, A. G. Hart, G. M. von Hippel, R. R. Horgan and C. J. Monahan, Phys. Rev. Lett. **107**, 112002 (2011) [Erratum: Phys. Rev. Lett. **115**, 039901 (2015)].
- [5] T. C. Hammant, A. G. Hart, G. M. von Hippel, R. R. Horgan and C. J. Monahan, Phys. Rev. D **88**, 014505 (2013) [Erratum: Phys. Rev. D **92**, 119904 (2015)].
- [6] R. J. Dowdall *et al.* [HPQCD Collaboration], Phys. Rev. D **85**, 054509 (2012).
- [7] R. J. Dowdall *et al.* [HPQCD Collaboration], Phys. Rev. D **89**, 031502 (2014) [Erratum: Phys. Rev. D **92**, 039904 (2015)].
- [8] S. W. Herb *et al.*, Phys. Rev. Lett. **39**, 252 (1977).
- [9] J. J. Aubert *et al.* [E598 Collaboration], Phys. Rev. Lett. **33**, 1404 (1974).
- [10] J. E. Augustin *et al.* [E598 Collaboration], Phys. Rev. Lett. **33**, 1406 (1974).
- [11] M. E. Peskin and D. V. Schroeder, *An Introduction to Quantum Field Theory* (Addison-Wesley, 1995).

- [12] N. Brambilla, *Nonrelativistic Effective Field Theories for Near Threshold States*, lectures presented at Summer School on Methods of Effective Field Theory and Lattice Field Theory, June 2017.
- [13] C. Gatttringer and C. B. Lang, *Quantum Chromodynamics on the Lattice: An Introductory Presentation* (Springer, 2010).
- [14] B. A. Thacker and G. P. Lepage, Phys. Rev. D **43**, 196 (1991).
- [15] C. Patrignani *et al.* [Particle Data Group], Chin. Phys. C **40**, 100001, (2016).
- [16] K. Seth, EPJ Web of Conferences **3**, 07006 (2010).
- [17] B. Aubert *et al.* [BaBar Collaboration], Phys. Rev. Lett. **101**, 071801 (2008) [Erratum: Phys. Rev. Lett. **102**, 029901 (2009)].
- [18] B. A. Kniehl, A. A. Penin, A. Pineda, V. A. Smirnov and M. Steinhauser, Phys. Rev. Lett. **92**, 242001 (2004) [Erratum: Phys. Rev. Lett. **104**, 199901 (2010)].
- [19] R. Mizuk *et al.* [Belle Collaboration], Phys. Rev. Lett. **109**, 232002 (2012).
- [20] E. Braaten, *Introduction to the NRQCD Factorization Approach to Heavy Quarkonium*, talk given at 3rd International Workshop on Particle Physics Phenomenology, November 1996, hep-ph/9702225.
- [21] W. E. Caswell and G. P. Lepage, Phys. Lett. **167B**, 437 (1986).
- [22] G. P. Lepage and B. A. Thacker, Nucl. Phys. Proc. Suppl. **4**, 199 (1988).
- [23] G. P. Lepage, *How to Renormalize the Schrödinger Equation*, lectures given at the VIII Jorge Andre Swieca Summer School, February 1997, nucl-th/9706029.
- [24] G. P. Lepage, L. Magnea, C. Nakhleh, U. Magnea and K. Hornbostel, Phys. Rev. D **46**, 4052 (1992).

- [25] A. Pineda, Prog. Part. Nucl. Phys. **67**, 735 (2012).
- [26] G. T. Bodwin, E. Braaten and G. P. Lepage, Phys. Rev. D **51**, 1125 (1995) [Erratum: Phys. Rev. D **55**, 5853 (1997)].
- [27] A. V. Manohar, Phys. Rev. D **56**, 230 (1997).
- [28] T. Becher and K. Melnikov, Phys. Rev. D **66**, 074508 (2002).
- [29] S. Weinberg, *The Quantum Theory of Fields: Vol. 1, Foundations*, (Cambridge University Press, 2005).
- [30] V. B. Berestetskii, E. M. Lifshitz and L. P. Pitaevskii, *Quantum Electrodynamics: Vol. 4*, (Butterworth-Heinemann, 1982).
- [31] D. J. Griffiths, *Introduction to Quantum Mechanics*, (Cambridge University Press, 2016).
- [32] A. Kvitsinsky, Journal of Physics A: Mathematical and General **25**, 1 (1992).
- [33] G. S. Bali and P. Boyle, Phys. Rev. D **59**, 114504 (1999).
- [34] E. Hairer, S. P. Nørsett, and G. Wanner, *Solving Ordinary Differential Equations I: Nonstiff Problems*, (Springer, 2010).
- [35] R.J. Hill and G.P. Lepage, Phys. Rev. D **62**, 111301 (2000).
- [36] C. T. H. Davies *et al.* [HPQCD Collaboration], PoS LATTICE **2013**, 438 (2014).
- [37] B. Aubert *et al.* [BaBar Collaboration], Phys. Rev. Lett. **103**, 161801 (2009).
- [38] G. Bonvicini *et al.* [CLEO Collaboration], Phys. Rev. D **81**, 031104 (2010).

Appendix A

Feynman Rules of NRQCD

The following are the relevant Feynman rules for this thesis, originally given in ref. [25].

We choose the momentum flow direction to be from left to right.

Heavy quark/antiquark propagator:



$$\frac{i}{k_0 - \frac{\mathbf{k}^2}{2m_q} + i\epsilon}$$

Logitudinal gluon propagator (Feynman gauge):



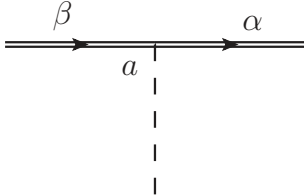
$$\frac{i}{k^2 + i\epsilon}$$

Transverse gluon propagator (Feynman gauge):



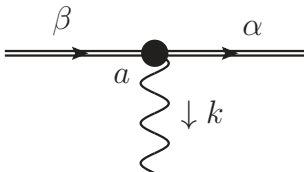
$$-\frac{i}{k^2 + i\epsilon}$$

Coulomb vertex:



$$-igT_{\alpha\beta}^a$$

Fermi vertex:



$$\frac{c_F g}{2m_q} (\boldsymbol{\sigma} \times \mathbf{k}) T_{\alpha\beta}^a$$

Appendix B

Spin-Dependent Coulomb NRQCD Amplitudes

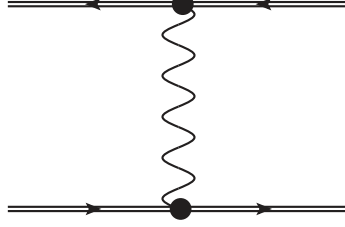
To study the hyperfine splitting in heavy quarkonium, we will consider the spin-dependent NRQCD amplitudes at tree-level and one-loop. We will perform the calculation in the Feynman gauge, with expressions for the gluon propagator given in Appendix A. As we are looking for binding energy effects, we perform the calculation in the potential region of scales, where if $k = (k_0, \mathbf{k})$ is the loop momentum,

$$k_0 \sim m_q v^2, \quad |\mathbf{k}| \sim m_q v$$

As we are considering the colorless heavy quarkonium, we also project all operators onto the color-singlet state, effectively replacing colour factors as $(T^a T^b)_{\alpha\beta} \rightarrow C_F$ [25].

B.1 Tree-Level

The tree-level diagram with a spin-flip operator looks like



The NRQCD Feynman rules in Appendix A give

$$i\mathcal{M} = C_F \left(\frac{c_F g}{2m_q} \right)^2 \frac{i}{q^2} \psi^\dagger(\boldsymbol{\sigma} \times \mathbf{q}) \psi \chi_c^\dagger(\boldsymbol{\sigma} \times \mathbf{q}) \chi_c$$

where $q = (q_0, \mathbf{q})$ is the 4-momentum transfer and the $i\eta$ prescription is neglected since we are at tree-level. We can simplify the fermion line by remembering that

$$\epsilon^{ikl} \epsilon^{imn} = \delta^{km} \delta^{ln} - \delta^{kn} \delta^{lm}$$

The fermion line then becomes

$$\psi^\dagger(\boldsymbol{\sigma} \times \mathbf{q}) \psi \chi_c^\dagger(\boldsymbol{\sigma} \times \mathbf{q}) \chi_c = \mathbf{q}^2 \psi^\dagger \boldsymbol{\sigma} \psi \chi_c^\dagger \boldsymbol{\sigma} \chi_c - q_k q_m \psi^\dagger \sigma_k \psi \chi_c^\dagger \sigma_m \chi_c$$

As we are interested in the expectation value of this operator for $1S$ states, we can make the replacement $q_k q_m \rightarrow \frac{1}{3} \mathbf{q}^2 \delta_{km}$ due to spherical symmetry. Thus, the amplitude becomes

$$\mathcal{M} = \frac{2\pi}{3} \frac{C_F \alpha_s}{m_q^2} \frac{\mathbf{q}^2}{q_0^2 - \mathbf{q}^2} \psi^\dagger \boldsymbol{\sigma} \psi \chi_c^\dagger \boldsymbol{\sigma} \chi_c$$

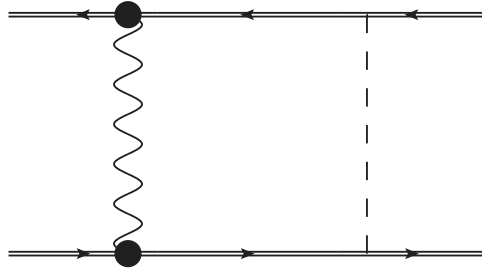
where $c_F \rightarrow 1$ is allowed to leading order in α_s . Our final step comes from remembering that we are interested in the potential regions of scales, so that the ratio $\frac{q_0}{\mathbf{q}}$ is suppressed

by a power of v . Our final result for the tree-level spin-dependent amplitude is then

$$\mathcal{M} = -\frac{2\pi}{3} \frac{C_F \alpha_s}{m_q^2} \psi^\dagger \boldsymbol{\sigma} \psi \chi_c^\dagger \boldsymbol{\sigma} \chi_c$$

B.2 One-Loop

We now consider the next-to-leading order contribution coming from the symmetric one-loop diagrams



Since the matching procedure is independent of the kinematical details of the quarkonium system, we will perform this calculation in its rest frame so that the momentum transfer vanishes. We further perform the calculation at the system's threshold, so that the kinetic energy vanishes. As the lattice NRQCD propagators generate $\mathcal{O}(a^2)$ terms in the continuum limit, and we are interested in linear dependence on a only, it is sufficient to compute the one-loop diagram with the continuum NRQCD propagators given in Appendix A. We can use our tree-level diagram to simplify the calculation:

$$\mathcal{M} = g^2 \frac{4\pi}{3} \frac{C_F^2 \alpha_s}{m_q^2} \psi^\dagger \boldsymbol{\sigma} \psi \chi_c^\dagger \boldsymbol{\sigma} \chi_c \int_* \frac{d^3 \mathbf{k}}{(2\pi)^3} \frac{1}{\mathbf{k}^2 + \lambda^2} \int \frac{dk_0}{2\pi i} \frac{i}{k_0 - \frac{\mathbf{k}^2}{2m_q} + i\eta} \frac{i}{-k_0 - \frac{\mathbf{k}^2}{2m_q} + i\eta}$$

where we added a gluon mass λ to regulate the Coulomb IR divergence, as well as neglected the energy component in the longitudinal gluon propagator as we are in the potential region of scales. The star on the momentum integral is a reminder to integrate up to the border of the first Brillouin zone. Performing the energy integral using the residue

theorem, we have

$$\mathcal{M} = -\frac{2}{3\pi} \frac{C_F^2 \alpha_s^2}{m_q} \psi^\dagger \boldsymbol{\sigma} \psi \chi_c^\dagger \boldsymbol{\sigma} \chi_c \int_* \frac{d^3 \mathbf{k}}{(\mathbf{k}^2 + \lambda^2)^2}$$

We can now perform the momentum integral over a spherically symmetric lattice with lattice spacing a :

$$\begin{aligned} \int_* \frac{d^3 \mathbf{k}}{(\mathbf{k}^2 + \lambda^2)^2} &= \int_0^{\pi/a} d|\mathbf{k}| \frac{4\pi \mathbf{k}^2}{(\mathbf{k}^2 + \lambda^2)^2} \\ &= \frac{\pi^2}{\lambda} - 4a + \mathcal{O}(a^3) \end{aligned} \tag{B.1}$$

The first term corresponds to the Coulomb singularity in agreement with eq. (2.11), while the second term is the contribution from the UV cut-off. Correspondingly using the $\mathcal{O}(v^4)$ heavy quark propagator

$$S(k) = \frac{1}{k_0 - \frac{\mathbf{k}^2}{2m_q} + \frac{\mathbf{k}^4}{8m_q^3}}$$

gives an additional correction to the second term:

$$\begin{aligned} \int_* \frac{d^3 \mathbf{k}}{(\mathbf{k}^2 + \lambda^2)^2} \left[1 - \frac{1}{1 - \frac{\mathbf{k}^2}{4m_q}} \right] &= - \int_0^{\pi/a} d|\mathbf{k}| \frac{\pi}{m_q^2 - \frac{\mathbf{k}^2}{4}} \\ &= -4a + \mathcal{O}\left(\frac{1}{m_q}\right) \end{aligned}$$

which multiplies the second term in eq. (B.1) by a factor of two. We see that including the relativistic correction doubles the value of the lattice artifact, which is expected as higher-dimension operators in the NRQCD Lagrangian are more sensitive to the UV momentum region [3]. The result for the Coulomb contribution to the 1-loop lattice NRQCD amplitude is then

$$\mathcal{M} = \frac{C_F \alpha_s^2}{m_q^2} \left[-\frac{2\pi m_q}{3\lambda} C_F + \frac{16C_F}{3\pi} a m_q \right] \psi^\dagger \boldsymbol{\sigma} \psi \chi_c^\dagger \boldsymbol{\sigma} \chi_c + \mathcal{O}(a^3)$$

Appendix C

Solving the Schrödinger Equation on the Lattice

We are interested in solving the time-independent Schrödinger equation for heavy quarkonium with reduced mass $\mu = m_q/2$. In natural units, this is given by

$$\left[\frac{1}{2\mu} \nabla^2 + \frac{C_F \alpha_s}{r} + E \right] \psi(\mathbf{r}) = 0 \quad (\text{C.1})$$

where ψ is the wave function, E is the energy of the bound state, α_s is the strong coupling constant and $C_F = 4/3$ is a colour factor arising from the $SU(3)$ gauge group. Let us dedimensionalize eq. (C.1) by working in distance units of the Bohr radius $r_b = 2/m_q C_F \alpha_s$:

$$\nabla^2 \psi(\mathbf{r}) = -2 \left(E + \frac{1}{r} \right) \psi(\mathbf{r})$$

where we shifted the energy $E \rightarrow (m_q C_F^2 \alpha_s^2) E/2$ as to make it dimensionless. Let us now make the following ansatz for the wave function, remembering that the potential is central:

$$\Psi(r) = \frac{u(r)}{r} \Theta(\theta) \Phi(\phi)$$

where the choice in radial dependence anticipates the Coulomb singularity at the origin. This choice leads to three different equations:

$$\begin{aligned}\frac{d^2\Phi}{d\phi^2} &= -m_l^2\Phi \\ \sin\theta\frac{d\Theta}{d\theta}\left(\sin\theta\frac{d\Theta}{d\theta}\right) &= [m_l^2 - l(l+1)\sin^2\theta]\Theta \\ \frac{d^2u}{dr^2} &= \left[\frac{l(l+1)}{r^2} - 2\left(\frac{1}{r} + E\right)\right]u\end{aligned}\tag{C.2}$$

where m_l and l are complex numbers *a priori*. The solution to the first two equations are the spherical harmonics given by

$$Y_l^{m_l}(\theta, \phi) = (-1)^{m_l} \sqrt{\frac{2l+1}{4\pi} \frac{(l-m_l)!}{(l+m_l)!}} P_l^{m_l}(\cos\theta) e^{im_l\phi}\tag{C.3}$$

where m_l and l are integers such that $l \geq |m_l|$ and $P_l^{m_l}(x)$ are the associated Legendre polynomials [31]. If we are interested in spherically symmetric solutions, then we must choose $l = m_l = 0$ to avoid any angular dependence. Thus, the angular part is simply $Y_0^0(\theta, \phi) = \frac{1}{\sqrt{4\pi}}$. The exact solution to the radial equation (C.2) with $l = 0$ is then

$$u(r) = 2r e^{-r}, \quad E = -\frac{1}{2}\tag{C.4}$$

We would now like to solve the Schrödinger equation on a spherically symmetric lattice, obtained by discretizing the radial equation (C.2). This is done by setting up a one-dimensional grid with lattice spacing a so that $r_n = na$, $n = 0, 1, 2, \dots$ and discretizing the second derivative using the central difference

$$a^2 u''(r) \rightarrow u(n+2) - 2u(n+1) + u(n) + \mathcal{O}(a^4)$$

so that the lattice Schrödinger equation, to $\mathcal{O}(a^4)$ is reduced to

$$u(n+1) - 2u(n) + u(n-1) + 2a^2 \left(\frac{1}{na} + E \right) u(n) = 0 \quad (\text{C.5})$$

for $n = 1, 2, \dots$ and the boundary condition is $u(0) = 0$. The difference equation can now be solved in two different ways.

C.1 Numerical Approach

The difference equation can be solved numerically by solving for $u(n)$ explicitly in an iterative process

$$u(n-1) = 2 \left[1 - a^2 \left(\frac{1}{na} + E \right) \right] u(n) - u(n+1) + \mathcal{O}(a^4) \quad (\text{C.6})$$

where $n = 1, \dots, n_{\max}$. This is done by the Numerov or “shooting” method [31]. Using the analytical solution eq. (C.4), we can set two successive values at a sufficiently large distance for the radial solution, as well as the initial energy guess, and eq. (C.6) builds the function $u(n)$ backwards to $r = 0$. For our purposes, we chose lattice spacings $a = 0.01 - 0.2$, and $r_{\max} \equiv n_{\max}a$ large enough so as to capture the full range of the wave function. Choosing r_{\max} to be an order of magnitude larger than the Bohr radius was enough for convergence of the results. We can then normalize the wave function using the trapezoidal rule:

$$1 \equiv \int_0^\infty dr |u(r)|^2 = \frac{a}{2} \left(u(0)^2 + 2 \sum_{n=1}^{n_{\max}-1} u(n)^2 + u(n_{\max})^2 \right) + \mathcal{O}(a^2)$$

For an inaccurate energy guess E_{guess} , $u(n)$ will blow up at the origin as the potential and kinetic energy will not be in balance. Therefore, a binary search in energy space should be performed until $|2 - u(n=0)| < \epsilon$, where ϵ is our desired tolerance. For our simulation

we performed the search with energy spacing $\Delta E = E_{\text{guess}}/10$ and a strict tolerance of $\epsilon = 10^{-7}$.

Our goal now is to use the Numerov method to determine the dependence of the bound state characteristics on the lattice spacing. Let us expand the binding energy and the radial wave function at the origin in a power series in the lattice spacing:

$$\begin{aligned} E &= E_c [1 + c_1 a + c_2 a^2 + \mathcal{O}(a^3)] \\ \Psi_l(0) &= \Psi_c(0) [1 + d_1 a + d_2 a^2 + \mathcal{O}(a^3)] \end{aligned} \tag{C.7}$$

where $E_c = -\frac{1}{2}$, $\Psi_c(0) = \frac{1}{\sqrt{\pi}}$. Once a solution $u(n)$ is determined, we are then ready to obtain the radial wave function by fitting our solution with the fit $A r e^{-B r}$, where $A = A(a)$ and $B = B(a)$ are fitting parameters with errors δA and δB respectively. Near the origin, the analytical radial wave function behaves like

$$\lim_{r \rightarrow 0} R(r) = \lim_{r \rightarrow 0} \frac{u(r)}{r} = 2$$

and so the radial wave function at the origin corresponds to the fit parameter A . Therefore, for a given lattice spacing a , the wave function at the origin is $A Y_0^0 = \frac{A}{\sqrt{4\pi}}$. We can now run our algorithm for multiple lattice spacings and fit the fit parameter $A(a)$ with a polynomial in a , while weighting each point by $\frac{1}{\delta A^2}$. We chose 20 lattice spacings in the range $0.01 - 0.2$ and obtained the values below for the expansion in eq. (C.7)

$$c_1 = d_1 = 0, \quad c_2 = d_2 = -\frac{1}{4} \tag{C.8}$$

We conjecture the exact form of both coefficients since our algorithm reproduced standard errors of $\mathcal{O}(10^{-5})$. Expanding to $\mathcal{O}(a^2)$, the square of the wave function at the origin is

$$|\Psi_l(0)|^2 = |\Psi_c(0)|^2 \left[1 - \frac{1}{2} a^2 + \mathcal{O}(a^4) \right]$$

Note that the wave function does not depend linearly on the lattice spacing. This is a result that follows from the central discretization of the Laplacian: a symmetric difference equation with global $\mathcal{O}(a^4)$ error results in local $\mathcal{O}(a^2)$ error, see ref. [34], Theorem 8.10. The theorem further states that the binding state characteristics should not depend on odd powers of the lattice spacing. However we were not able to confirm this fact reliably for powers greater than cubic, since there is a lack of stability as the order of the polynomial fit in a increases.

C.2 Analytical Approach

The difference equation (C.6) is also simple enough to be solved analytically, see ref. [32].

We simply quote the solution:

$$u(n) = \frac{2na}{(1+a^2)^{1/4}} \exp(-n \operatorname{arcsinh} a)$$

with energy given by

$$\begin{aligned} E_l &= -\frac{1}{a^2} [(1+a^2)^{1/2} - 1] \\ &= -\frac{1}{2} \left(1 - \frac{1}{4}a^2 + \frac{1}{8}a^4 + \mathcal{O}(a^6) \right) \end{aligned}$$

confirming the coefficients c_1 and c_2 in eq. (C.8). Then the lattice wave function is given by

$$\Psi_l(n) = \frac{1}{\sqrt{\pi}} \frac{1}{(1+a^2)^{1/4}} \exp(-n \operatorname{arcsinh} a) \quad (\text{C.9})$$

And the wave function at the origin is simply

$$\begin{aligned} |\Psi_l(0)|^2 &= |\Psi_c(0)|^2 \frac{1}{(1+a^2)^{1/2}} \\ &= |\Psi_c(0)|^2 \left(1 - \frac{1}{2}a^2 + \frac{3}{8}a^4 + \mathcal{O}(a^6) \right) \end{aligned}$$

confirming the coefficients d_1 and d_2 in eq. (C.8). We plot the numerical and analytical solutions for the wave function at the origin as a function of the lattice spacing in Figure C.1, and see perfect agreement between the two approaches. Note that both the energy and lattice wave function at the origin only depend on even powers of a , as expected from ref. [34].

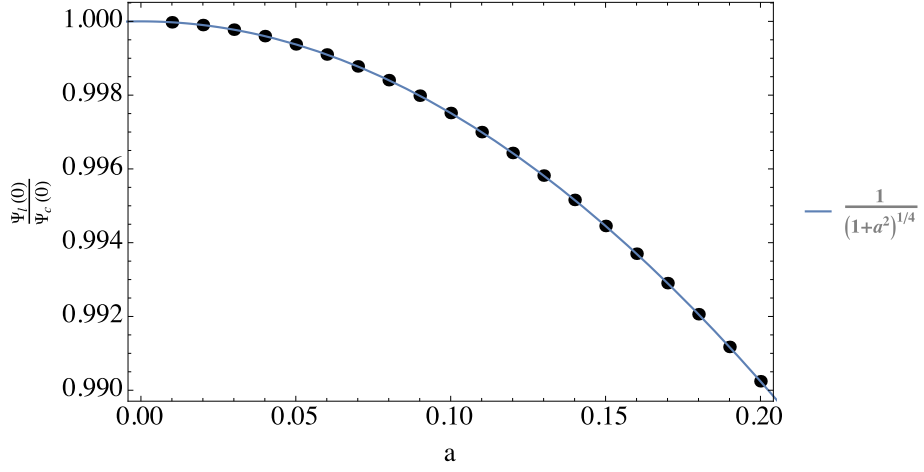


Figure C.1: Plot of the wave function at the origin as a function of lattice spacing normalized by the continuum solution $\Psi_c(0) = \pi^{-1/2}$ in units of the Bohr radius. The black dots label the numerical solution for lattice spacings $a = 0.01 - 0.2$, while the blue line indicates the analytical solution eq. (C.9).